An Evaluation of Control Strategies: Disturbance Sensitivity Study with an Enhanced Underwater Vehicle Model

Eric Conrado de Souza
E-mail: eric.souza@poli.usp.br

Newton Maruyama
E-mail: maruyama@usp.br

Av. Prof. Mello Moraes n°2231, Depto. de Engenharia Mecatrônica e de Sistemas Mecânicos, Escola Politécnica, Universidade de São Paulo, 05508-900, São Paulo, SP, Brasil

Abstract: *This paper is concerned with the comparison of closed-loop performance characteristics of underwater vehicles undertaking standard mission activities. The comparison of closed-loop performance encompasses issues with respect to the propulsion and navigation systems, to disturbance rejection, and input tracking. Our evaluations consider the use of a linear PID feedback, a PI feedforward and a robust control strategies applied to a full order vehicle model. We show that much of the performance deterioration may be attributed mainly to cable inertia. We also verify that the robust control strategy does not necessarily allow for better performance over the linear feedback control strategies implemented when vehicle motions are confined to low velocity values. These and other partial results will aid the design of the control system for an underwater vehicle currently under construction.*
Keywords: *Mobile robots, Nonlinear control systems*

Introduction

This paper focuses its attention on a number of issues regarding performance aspects encountered when control strategies are applied to Unmanned Underwater Vehicles (UUVs) which alone is characterized by complicated nonlinear and coupled dynamics. The system complexity increases considerably when the vehicle propulsion system, tether cable and navigation system also pertain to the vehicle model.

We intend to consider a worst case situation in which various sources of disturbances and model perturbations are present, for example: In our case scenario the vehicle is linked to a surface support vessel through the tether cable while performing a specified task maneuver. Thus, the adopted control strategy should not only compensate for the cable unstructured disturbances, when present, but also for other structured perturbations, such as current velocity, the vehicle parametric variations (e.g. added mass), and unmodeled dynamics. For this intent, we investigate and implement three positioning control techniques. The first is a decentralized linear PID strategy. The second one is a feedforward control technique. The third one is characterized by nonlinear discontinuous terms, the sliding mode robust control (Yoerger and Slotine, 1985).

This text is organized as follows. Vehicle modeling is addressed in Section 3. A brief overview of the control strategies is then presented in Section 4. The next section discusses fundamental issues such as performance and computational implementation and some results are depicted. Finally concluding remarks are drawn based on what has been presented.

Nomenclature

$\hat{M}_\Delta$ = estimated vehicle inertia matrix with only diagonal elements and vehicle mass m ($\hat{M}_\Delta \in \mathbb{R}^{6\times 6}$);
ν = vehicle velocity vector in body coordinate system ($\nu \in \mathbb{R}^6$);
ν_c = sea current velocity in body coordinate system ($\nu_c \in \mathbb{R}^6$);
$\eta = [x, y, z, \phi, \theta, \psi]^T$ = vehicle position with respect to inertial reference system ($\eta \in \mathbb{R}^6$);
τ = vehicle control vector defined in body coordinate system ($\tau \in \mathbb{R}^6$).

Vehicle Modeling

The vehicle model used for the model based control synthesis is the MURS 300 Mark II[a] Vehicle (Ishidera et al., 1986). The MURS vehicle is nearly neutrally buoyant and controllable on all six degrees of freedom, *dof*, containing six thrusters distributed longitudinally two by two on each body axis. A full order mathematical model has been developed, i.e., all six (d.o.f.) are considered. A standard and well established general expression describing the underwater vehicle dynamics may be formulated according to the nonlinear and multivariable

[a] Mitsui Ocean Development & Engineering Co., Ltd.

representation (Kalske and Happonen, 1991; Fossen, 1994; Souza, 2003):

$$M\dot{\nu} + C(\nu)\nu + F_D(\nu_r) + G(\eta) = \tau_{prop} + \tau_c + \tau_{cable}, \tag{1}$$

$$\dot{\eta} = J(\eta)\nu. \tag{2}$$

The mass matrix M accounts for vehicle inertia and added mass while the centripetal and Coriolis force matrix C is derived from the rigid body dynamic expressions and also includes centripetal and Coriolis added mass forces and moments. The term $F_D(\nu_r)$ stands for nonlinear hydrodynamic damping action (drag). The relative velocity term ν_r is used to describe the vehicle velocity relative to the water motion, or current, as:

$$\nu_r = \nu - \nu_c. \tag{3}$$

Note that unlike constant parameter modeling of hydrodynamic drag forces (see (Yoerger and Slotine, 1985; Fossen, 1994; Souza and Maruyama, 2003)) we've adopted a varying parameter drag model, as this can provide for a more realistic vehicle dynamics description. Restoring forces and moments are accounted for in $G(\eta)$, comprising gravitational weight and buoyancy components. The tether cable disturbance forces are represented by τ_{cable}. Because the result of wind, wind generated waves and tide becomes gradually less with depth the most important environmental effect, when operating activities are conducted at high depths at sea, is the current. Therefore other environmental fenomena are not considered. The current disturbance is considered in τ_c. The J matrix indicates when coordinate transformation is made between the inertial and mobile reference coordinate frames.

Modeling of the Propulsion System

Thrusters dynamics can be responsible for the incorporation of lags and nonlinearities to the system for which the controller may not be able to compensate for. Their dynamics may be composed of two distinct sources: hydrodynamics of the interaction of the propeller blades and water, and the dynamics of the electrical DC or brushless motor, considered negligible. The thrusters hydrodynamic representation follows according to the two state model described in (Healey et al., 1995), where the propeller revolution n and fluid flux velocity U_a are related by lift and damp expressions. The controller output signal are mapped to each thruster through the static propulsion T and propeller revolution n relationship:

$$T = b(n, U_a)n|n|, \tag{4}$$

which leads to the mapping:

$$\tau = B(b(n, U_a))\mathbf{u}, \quad B \in \mathbb{R}^{6\times 6}, \tag{5}$$

where $\mathbf{u}$ is defined as the control variable and the matrix B maps the controller output signals to each thrusters.

We considered an internal or electrical motor propeller revolution loop control for each thruster, which auxiliates disturbance rejection relative to hydrodynamic loads. It is assumed that the motor shaft velocity is provided by a tachogenerator.

Tether Cable Modeling

The tether cable dynamics has been incorporated into the controlled system model. The cable is modeled according to the lumped mass procedure (Nomoto and Hattori, 1986; Yokobiki et al., 2000; Driscoll et al., 2000), augmented to incorporate internal damping terms. The cable lower end is considered connected to the center of the vehicle reference system. The tether cable modeling procedure considered a three dimensional model, where flexural-torsional effects were neglected. The tether 3D dynamics, considering each discrete element, may be summarized by the following:

$$\left[M_i + M_{Ai}\right]_{cable} \ddot{\eta}_{cable_i} = (T_i + P_i)_{cable} - (T_{i-1} + P_{i-1})_{cable} + F_i, \tag{6}$$

where $\ddot{\eta}_{cable_i}$ is the acceleration vector of the i-th node, and M_i, $M_{A_i} \in \mathbb{R}^3$ represent the mass and added mass of the i-th cylindrical element, see (Yokobiki et al., 2000) for details. In the above expression we also have N_{cable} as the total number of nodes used and $i = 1..N_{cable} - 1$.

Internal Forces

The axial tension and internal damping forces over each discrete cable element may be modeled as a mass-spring-damper system, as observed by Fig. 2(b). In this configuration T_{cable_i} stands for the axial tension acting on the i-th node, Fig. 3(a), and may be expressed as:

$$T_{cable_i} = E\frac{A_{cable_i}}{l_{0_i}}\mathbf{R_i}\left[\mathbf{1} - \frac{\mathbf{l_{0_i}}}{|\mathbf{R_i}|}\right]. \tag{7}$$

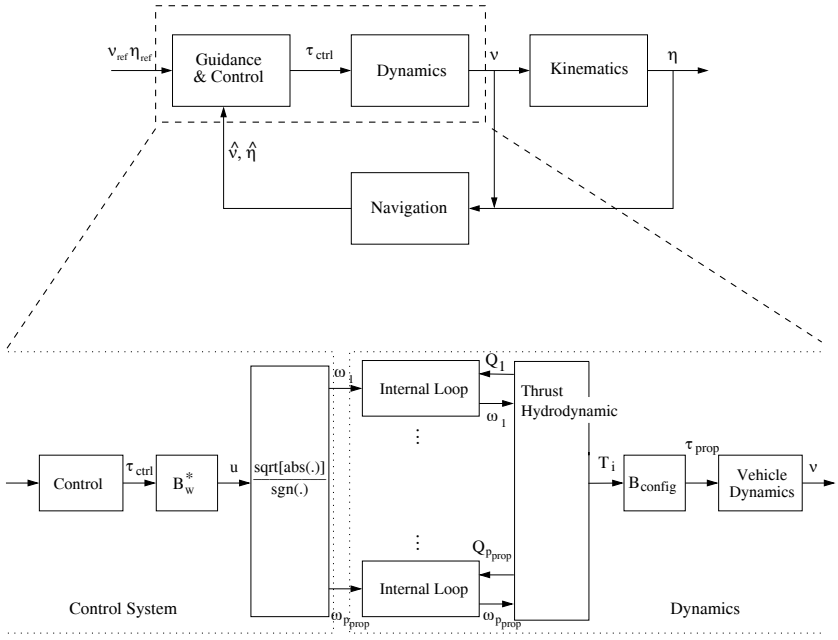

Figure 1. Block diagram schematically showing how the controller output signal τ is transformed into physical control effort, considering a propeller velocity n feedback control.

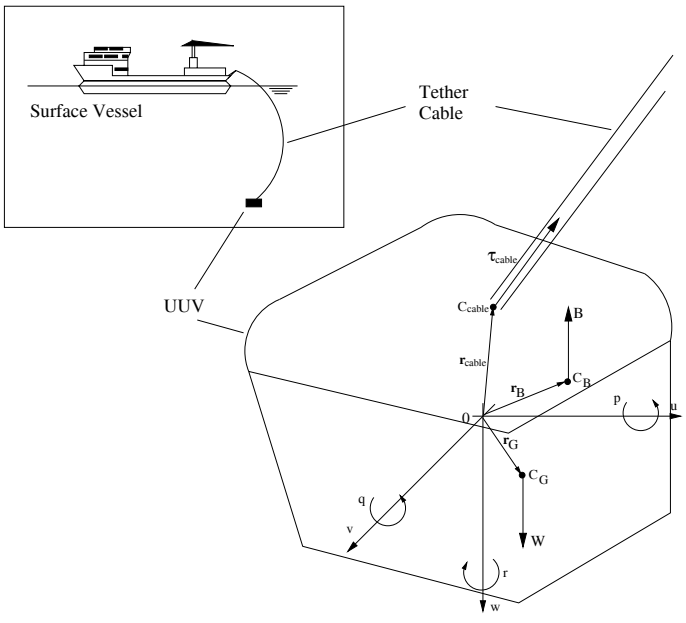

(a) Underwater vehicle connected to a surface support vessel.

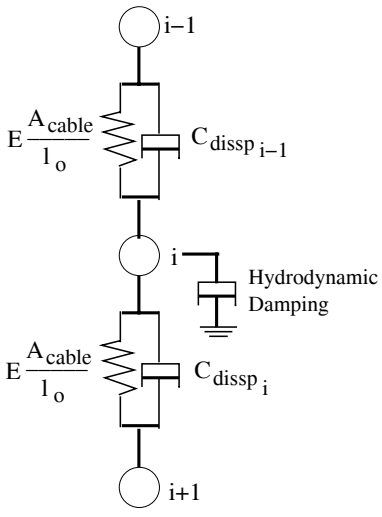

(b) Tether cable dynamics: analogy to a mass-spring-damper system.

Figure 2. Vehicle tether cable and modeling analogy.

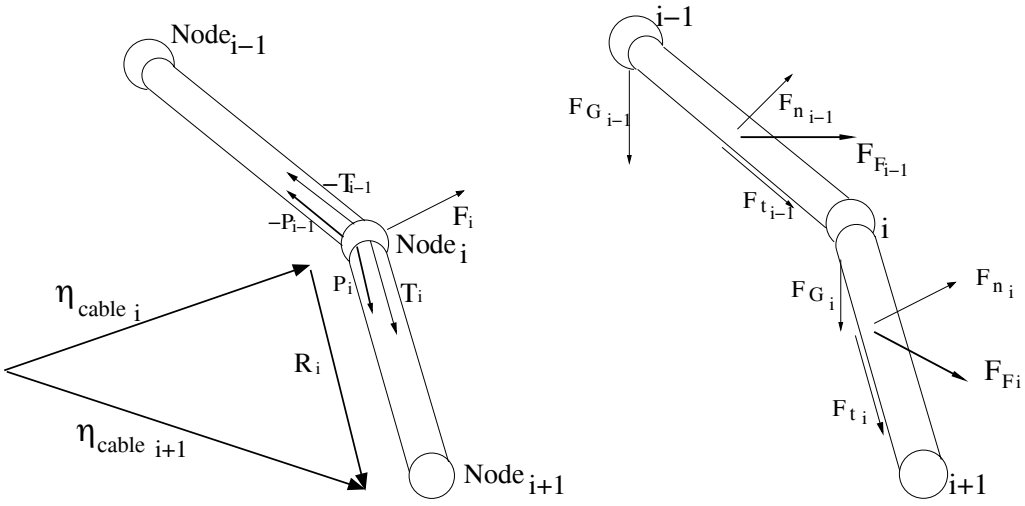

(a) Discrete cylindrical elements and internal forces.

(b) External forces relative to each cable node.

Figure 3. Vehicle tether cable modeling.

In the above expression E is the cable Young modulus, A_{cable_i} corresponds to the cable cross section area, with cable diameter d_i, and l_{0_i} as the unstretched cable element length. The distance vector $\mathbf{R_i}$ is given by:

$$\mathbf{R_i} = (\eta_{cable_{i+1}} - \eta_{cable_i}). \tag{8}$$

where η_{cable_i} is the position of the i-th node.

The existing friction between the core conductor insulation with the internal layer of the outer cable protection covering is responsible for a damping effect. This damping action is assumed linear and modeled as proportional to the difference of velocities of two consecutive cable nodes (Buckham et al., 1999):

$$P_i = C_{cable}\left[(\dot{\eta}_{cable_i} - \dot{\eta}_{cable_{i-1}})\frac{\mathbf{R_i}}{|\mathbf{R_i}|}\right]\frac{\mathbf{R_i}}{|\mathbf{R_i}|}. \tag{9}$$

External Forces

The external resultant F is the result of both restoring F_G and hydrodynamical damping F_F forces:

$$F_i = \frac{1}{2}(F_{F_i} + F_{F_{i-1}}) + F_{G_i}. \tag{10}$$

The hydrodynamical force F_F may be decomposed into normal and tangential components yielding to the following equation:

$$F_{F_i} = F_{n_i} + F_{t_i} = \frac{1}{2}\rho d_i(C_n U_{n_i}|U_{n_i}| + C_t U_{t_i}|U_{t_i}|)|\mathbf{R_i}|. \tag{11}$$

The water specific mass is represented by the constant ρ, and C_n e C_t are the normal and tangential damping coefficients, usually considered constant. The remaining terms, U_{n_i} e U_{t_i}, stand for the normal and tangential velocity components of the fluid flow for each cable element. These are evaluated according to:

$$U_{t_i} = \frac{[(\dot{\eta}_c - \dot{\eta}_{cable_i})\mathbf{R_i}]\mathbf{R_i}}{|\mathbf{R_i}|^2}, \tag{12}$$

$$U_{n_i} = \dot{\eta}_c - \dot{\eta}_{cable_i} - U_{t_i}, \tag{13}$$

where $\dot{\eta}_c$ corresponds to the current velocity, as stated before.

Dynamic Positioning Strategies

According to Eq. 1 the vehicle dynamics is characterized by the coupling of all d.o.f. state variables. Nevertheless a SISO control design methodology was applied, where Eq. 1 is first transformed into a set of six uncoupled

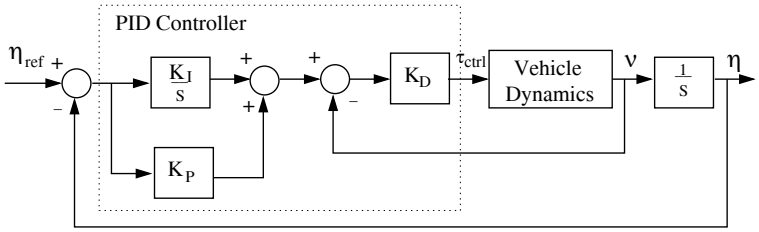

Figure 4. Control system block diagram for the linear PID strategy.

nonlinear system equations, by leaving out, i.e. neglecting, all state coupling terms. Each SISO equation, corresponding to a single degree of freedom model, is then linearized about a nominal operation point. Consider, for example, the simplified (uncoupled) surge motion dynamics representation be of the form:

$$\dot{u} = \frac{X_u}{(m - X_{\dot{u}})} u + \frac{X_{u|u|}}{(m - X_{\dot{u}})} u|u| + \frac{1}{(m - X_{\dot{u}})} \tau, \tag{14}$$

where $X_{(.)}$ denotes dynamical parameters dependent on the vehicle velocity and acceleration. Applying Taylor's series expansion and linearizing Eq. 14 leads to:

$$\dot{u}_\delta = a(u^*) u_\delta + b \tau_\delta, \tag{15}$$

where:

$$a(u^*) = \frac{X_u + 2X_{u|u|}u^*}{(m - X_{\dot{u}})} \text{ and } b = \frac{1}{(m - X_{\dot{u}})}. \tag{16}$$

Transforming Eq. 15 to the Laplace domain yields to an open loop (o.l.) transfer functions with a single pole dependence:

$$G_{ol}(s) = \frac{b}{s - a}. \tag{17}$$

Restoring forces are also not considered in the design procedure, although they may be feedforwarded by the controller if necessary. Under the circumstances considered below, however, this procedure was found not to be necessary.

As stated before, three different positioning strategies are chosen for implementation, comparison, and assessment of their results. For the sake of brevity, however, the control strategies implemented in this study will not be described in details. Emphasis is given to results and their analysis. We suggest the interested reader to refer to the references (Souza, 2003; Souza and Maruyama, 2003) and the references therein for a more thorough explanation of the control techniques under consideration.

Linear PID Control

The EAVE-EAST linear PID structure (Fossen, 1994) is implemented by considering a decentralized design. The controller parameters are determined so the closed loop system dynamics is dictated by two dominant complex poles. This is carried out by applying pole assignment formulae to Eq. 17, for the surge motion, and to the other *dof*, see details in (Souza, 2003). The linear control law, with structure depicted in Fig. 4, is given by:

$$\tau_{PID}(s) = J^T(\eta) K_D \left(\frac{K_P s + K_I}{s} (\eta_{ref} - \eta) - \nu \right). \tag{18}$$

Feedforward Control Technique

This technique combines a feedforward compensation term with a feedback regulation term. Two distinct actions are employed to achieve velocity control. To begin with, a feedforward control signal based on the vehicle dynamical model and input (or desired) trajectories is applied by the controller. The linear compensating action is generated by a linear P-PI control technique, as described in (Cunha et al., 1994; Cunha et al., 1995) and depicted in Fig. 5. The linear control part, considering all *dof*, is determined according to the following:

$$\tau_{feedback}(s) = J^T(\eta) \left(\frac{K_{P1} s + K_I}{s} \right) [K_{P2}(\eta_{ref} - \eta) - \dot{\eta}]. \tag{19}$$

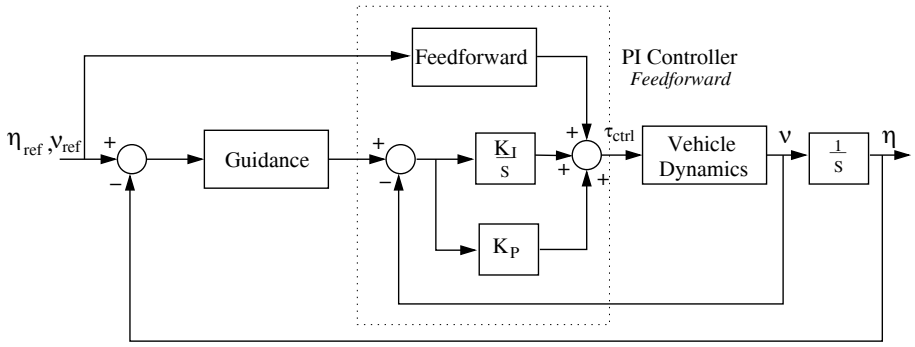

Figure 5. Control system block diagram for the P-PI with feedforward strategy.

Once again, the controller parameters where determined by applying pole assignment expressions to the design model. The overall control action may, thus, be written as:

$$\tau_{P-PI} = \tau_{feedforward} + \tau_{feedback}. \tag{20}$$

Sliding Mode Control

Design related theoretical background and methodology for the Sliding Mode strategy implemented and described here is based on the results of (Yoerger and Slotine, 1985; Slotine and Li, 1991)[b]. From Eq. 1 we define:

$$f(\nu, \eta, t) = -C(\nu)\nu - F_D(\nu) - G(\eta), \tag{21}$$

which, in turn, can be decomposed into a nominal component plus an associated uncertainty:

$$f(\nu, \eta, t) = \hat{f}(\nu, \eta, t) + \Delta f(\nu, \eta, t). \tag{22}$$

We define $d(t)$ as unmodeled dynamics (perturbations) and external disturbances. It is assumed that the uncertainty of $f(\nu, \eta, t)$ and $d(t)$ are bounded, that is:

$$F(\nu, \eta, t) \geq |\Delta f(\nu, \eta, t)| \text{ and } D(t) \geq |d(t)|. \tag{23}$$

By defining a tracking variable s:

$$s(t, \eta, \dot{\eta}) = \dot{\tilde{\eta}} + 2\lambda\tilde{\eta} + \lambda^2 \int_0^t \tilde{\eta} dr, \quad \tilde{\eta} = \eta - \eta_{ref} \tag{24}$$

a trajectory is established by the sliding surface $s = 0$ for the vehicle dynamics to follow. Although this condition does not mean that $\tilde{\eta} = 0$ at every instant the tracking error $\tilde{\eta}$ converges to zero when sliding mode is reached, i.e., when the vehicle dynamics slides the surface $s = 0$. In order to avoid chattering a boundary layer around the $s = 0$ surface with thickness Φ is adopted. While the vehicle dynamics remains "inside" this boundary layer no switching is made. If the region outside the layer is reached then switching is carried out. The control law is therefore:

$$\tau_{SM} = -f(\nu, \eta, t) - \hat{M}_\Delta[\lambda^2\tilde{\eta} + 2\lambda\dot{\tilde{\eta}} - \ddot{\eta}_{ref}] - K(\nu, \eta, t)sat(s/\Phi), \tag{25}$$

where:

$$K(\nu, \eta, t) = (\beta - 1)\hat{M}_\Delta|\lambda^2\tilde{\eta} + 2\lambda\dot{\tilde{\eta}} - \ddot{\eta}_{ref}| + F(\nu, \eta, t) + D(t), \tag{26}$$

where the symbol β stands for uncertainty of inertia elements and:

$$sat(s/\Phi) = \begin{cases} sgn(s/\Phi), \text{ if } |s/\Phi| \geq 1 \\ s/\Phi, \text{ otherwise} \end{cases}. \tag{27}$$

[b] An alternative and more robust approach to the sliding mode control can be found in: E. Bailey and A. Arapostathis (1987). Simple Sliding Mode Control Scheme Applied to Robot Manipulators, **International Journal of Control 45**(4):1197-1209. From a system stability point of view the control approach here adopted suffices in satisfying design requirements.

Table 1. Relative attenuation of the cable upper-end vertical motion and vehicle vertical and longitudinal motion amplitudes due to cable disturbance.

Control Strategy	Configuration 1:	Configuration 2:
P-PI *Feedforward*	60%	99%
PID	61%	99%
Sliding Mode Integral	82%	96%

Control Strategy	Configuration 1:		Configuration 2:	
	$x\ (m)$	$z\ (m)$	$x\ (m)$	$z\ (m)$
P-PI *Feedforward*	0.59	1.2	0.050	0.020
PID	0.500	1.15	0.060	0.030
Sliding Mode Integral	0.201	0.520	0.030	0.100

Simulation Results

Simulations were carried out under the MATLAB environment, where the vehicle dynamics are simulated at 1000Hz while the controller algorithm for all strategies runs at 10Hz. First order functions, with time constants approximately close to $5s$ for all d.o.f., are adopted as reference velocity trajectories. Maximum nominal desired velocities are considered equal to $[0.25; 0.25; 0.25]m/s$ and $[0; 0; 0.013]rad/s$ for linear and angular motions respectively. These trajectories are defined so that final relative position/attitude values achieve $[25m; 25m; 25m; 0rad; 0rad; 1.3rad]$ considering simultaneous motions for all d.o.f.. In addition, a constant $-[0.51; 0.51; 0.51]m/s$ current velocity profile is adopted, and defined in the inertial reference system.

The system is assumed to be fully observable, i.e., position and velocity measurements are available to be fed back to the controller. Signal measurement error, present in a real operating scenario, is modeled according to:

$$\text{Signal error} = bias_{sensor} + random_{sensor} + noise_{electronics}. \tag{28}$$

In our evaluations a constant bias component was assumed and considered negligible, since it can be compensated for once it is known. Random and noise signal error estimates were "borrowed" from (Hyland and Taylor, 1993), and which corresponds to measurements obtained from a Doppler/INS - *Doppler/Inertial Navigation System*, see (Lin, 1991) for details. Signal filtering was performed by 2nd order filters which, in turn, were responsible for the introduction of lags to the controlled system. This lag is directly related to each filter poles, and a tradeoff is verified between noise/signal attenuation and lag build up.

As expected, the surface support vessel is subject to wave and wind generated (induced) motions. Therefore, in order to approach the dynamical positioning problem of the UUV through a practical perspective it is interesting to evaluate the system behaviour with respect to the surface vessel motion. For this intent, as a second sensibility case study, we considered the tether cable upper end-point subject to a **vertical** sine-wave of $0.1Hz$ of frequency with a $3m$ peak-to-peak amplitude.

The results are shown in Fig. 6. These were obtained with the control laws described by Eqs. 18, 20 and 25, respectively. The cable disturbance attenuation results are summarized in Table 1.

Discussions and Concluding Remarks

From the results presented above it can clearly be seen that stabilization for surge, sway and heave positioning occurs in a very satisfactorily manner. Near zero steady state error can be observed for all controlled *dof*, i.e. all measured position trajectories indicate little or absence of position overshoot ($< 0.1m$) which is greatly desirable since physical contact with some other submerged object or facility could damage the vehicle or both, and jeopardize mission objectives. Note, also, that the cable and propulsion systems lags are compensated satisfactorily, thus disturbance rejecting is verified. It is important to stress out that due to the low inertia thrusters adopted the propulsion system did not contribute for an overall system performance deterioration.

As seen from the simulation results the developed trajectory profiles are characterized by noisy curves (in particular the velocity profiles of the sliding mode strategy, see Fig. 6(f)). Satisfactory signal filtering performance is not our primary concern other than to gain preliminary insight on the controlled system behaviour with respect to delay on state measurement-estimation as a filtering procedure could impose on real implementations.

It is noteworthy to mention that the performance-measurement error robust tradeoff was verified, that is, a compromise between performance measures[c] and measurement error rejection must be realized since good attendance of these is not achievable simultaneously. From (Souza, 2003) the results obtained from implementation

[c]Disturbance rejection, reference tracking, and insensitivity to the plant varying parameters.

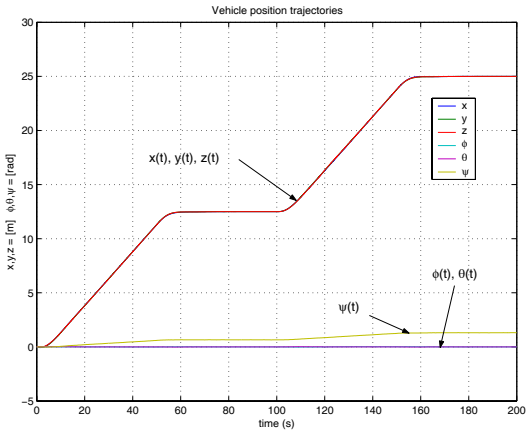

(a) Position tracking results for the PID strategy.

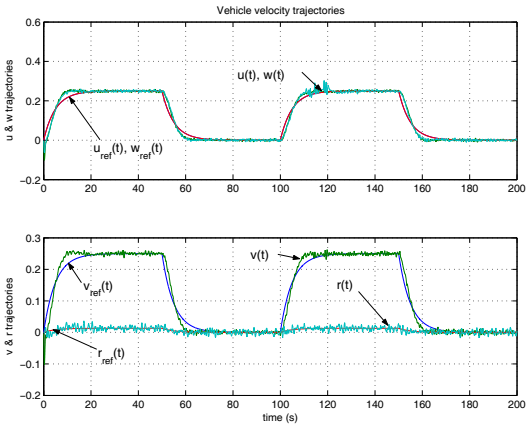

(b) Velocity tracking results for the PID strategy.

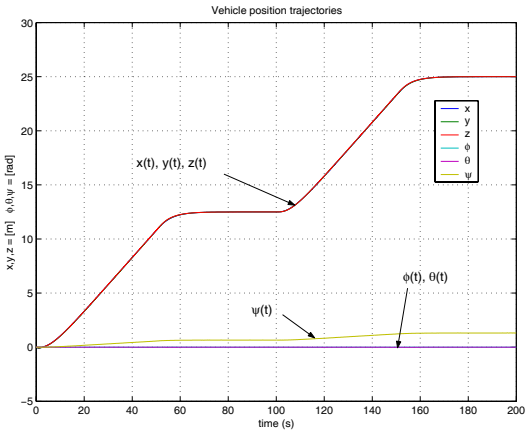

(c) Position tracking results for the PPI strategy.

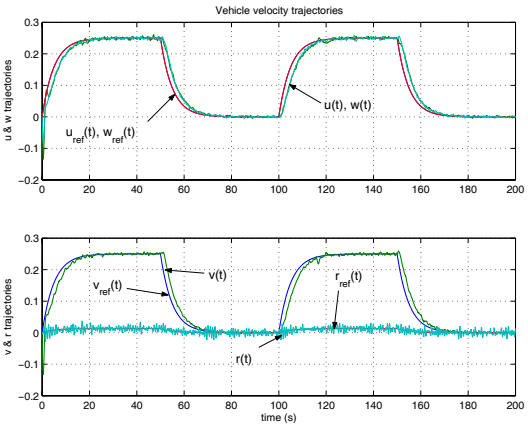

(d) Velocity tracking results for the PPI strategy.

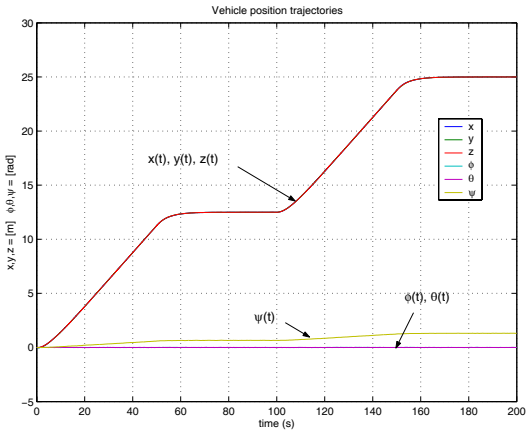

(e) Position tracking results for the SMI strategy.

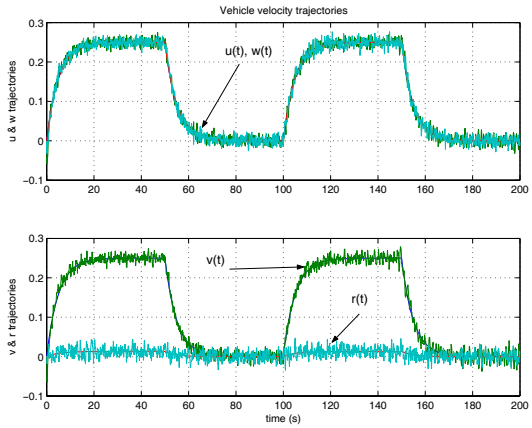

(f) Velocity tracking results for the SMI strategy.

Figure 6. Position and attitude tracking results vehicle without the tether cable model.

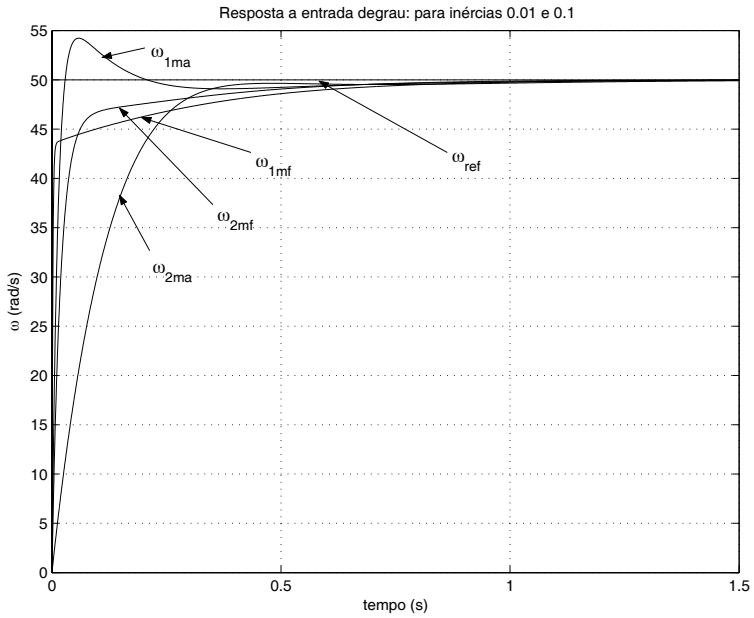

Figure 7. Closed and open loop comparison of time delay relative to a step input. Two thruster inertia values were used: $I_{prop_1} = 0.01kgm^2$ (curve "1") e $I_{prop_2} = 0.1kgm^2$ (curve "2"). The acronyms *ma* and *mf* indicate open-loop and closed-loop results, respectively.

of the control strategies considered therein indicate that best performance results could be obtained with the robust sliding mode control strategy, followed by the P-PI technique, and lastly with the linear PID strategy. As it can be seen from Fig. 6 the PID strategy allowed for superior results (with respect to measurement lags) as expected according to the performance and measurement error rejection tradeoff. The results of Figs. 6(e) and 6(f) indicate greater signal noise sensitivity of the robust sliding mode control strategy.

For the results presented above the controller parameters for the P-PI and the sliding mode control strategies were adjusted for a more modest performance scheme in order to cope with reasonable filtering lags. It is important, however, to note that performance specifications could be relaxed, thus allowing for a more satisfactory measurement error rejection result.

From the tether cable sensibility results it is possible to infer that with the cable physical properties defined by the *configuration 1* set (see Table 2) the sliding mode controlled system allowed for superior performance, suggesting a non-recommendation of the PID control strategies under the above simulating conditions. Alternatively, when the *configuration 2* cable properties set was considered equivalent vehicle performance results was verified for all control techniques. From these results we observe a very effective vertical motion attenuation (due mostly to the cable physical parameters rather than to the control strategies employed) and a significant induced horizontal motion. We may therefore conclude that the tether cable selection should be undertaken in regard to operational as well as environmental conditions.

The results presented above indicate that even under a considerable load of disturbances, which is expected in practical implementations, the control systems are able to satisfy performance specifications. We note, however, that tracking performance was achieved under "slow" desired dynamics (i.e. dynamic positioning), and further analysis is needed for "fast" dynamic performance. We may add that the cable represents, by far, the most important disturbance, responsible for lags and, when tensioned, demands most of the vehicle propulsion power. Further evaluation of these control strategies will be possible through experimental tests of an open-frame overactuated vehicle, currently under construction, through pool and open sea test trials.

Acknowledgements

The authors would like to thank for the sponsoring made by the Conselho Nacional de Desenvolvimento Científico e Tecnológico - CNPq and Financiadora de Estudos e Projetos - Finep.

References

Buckham, B., Nahon, M. and Seto, M. (1999). Three-Dimensional Dynamics Simulation of a Towed Underwater Vehicle, **Proceedings of the 18th Conference on Offshore Mechanics and Artic Engineering** pp. 1–8.

Table 2. Tether cable physical properties.

Parameters	**Configuration 1:** (Nomoto and Hattori, 1986)	**Configuration 2:** CTPETRO Program
Operational depth (m)	200	200
Cable length (m)	220	220
Cable diameter (mm)	30	12
Young modulus (N/m^2)	$1.372e^{10}$	$6.437e^{10}$
Weight in water (N/m)	1.87	3.77
Inner damping constant (Ns/m)	100	100
Number of discrete elements	40	40

Cunha, J. P. V. S., Costa, R. R. and Hsu, L. (1995). Design of a High Performance Variable Structure Position Control of ROV's, **IEEE Journal of Oceanic Engineering 20**(1): 42–55.

Cunha, J. P. V. S., Lizarralde, C. F., Costa, R. R., Hsu, L., Smith Jr., R., Wollmann Jr., D. and Sant'Anna, A. C. C. M. (1994). Sistema de Posicionamento Dinâmico para um Veículo Submarino de Operação Remota, **X Congresso Brasileiro de Automática** pp. 1309–1314.

Driscoll, F. R., Lueck, R. G. and Nahon, M. (2000). Development and Validation of a Lumped-Mass Dynamics Model of a Deep-Sea ROV System, **Applied Ocean Research 22**: 169–182.

Fossen, T. I. (1994). **Guidance and Control of Ocean Vehicles**, John Wiley & Sons.

Healey, A. J., Rock, S. M., Cody, S., Miles, D. and Brown, J. P. (1995). Toward an Improved Understanding of Thruster Dynamics for Underwater Vehicles, **IEEE Journal of Oceanic Engineering 20**(4): 354–361.

Hyland, J. C. and Taylor, F. J. (1993). Mine Avoidance Techniques for Underwater Vehicles, **IEEE Journal of Oceanic Engineering 18**(3): 340–350.

Ishidera, H., Tsusaka, Y., Ito, Y., Oishi, T., Chiba, S. and Maki, T. (1986). Simulation and Experiment Of Automatic Controlled ROV, **Proceedings of 5th International Offshore, Mechanical and Artic Engineering Symposium** pp. 260–267.

Kalske, S. and Happonen, K. (1991). Motion Simulation of Subsea Vehicles, **Proceedings of the 1st International Offshore and Polar Engineering Conference**, *Edinburgh, UK* **2**: 74–84.

Lin, C.-F. (1991). **Modern Navigation, Guidance, and Control Processing**, Vol. II of *Advanced Navigation, Guidance, and Control, and Their Applications*, Prentice Hall.

Nomoto, M. and Hattori, M. (1986). A Deep ROV "DOLPHIN 3K": Design and Performance Analysis, **IEEE Journal of Oceanic Engineering 11**(3): 373–391.

Slotine, J.-J. E. and Li, W. (1991). **Applied Nonlinear Control**, Prentice Hall.

Souza, E. C. (2003). **Modelagem e Controle de Veículos Submarinos Não Tripulados**, Dissertação (Mestrado), Escola Politécnica da Universidade de São Paulo.

Souza, E. C. and Maruyama, N. (2003). An Evaluation of Control Strategies Using an Enhanced Underwater Vehicle Model, **Proceedings of the 10th International Symposium on Dynamic Problems of Mechanics**, *Ubatuba, Brasil* pp. 29–34.

Yoerger, D. and Slotine, J.-J. E. (1985). Robust Trajectory Control of Underwater Vehicles, **IEEE Journal of Oceanic Engineering 10**(4): 462–470.

Yokobiki, T., Koterayama, W., Yamaguchi, S. and Nakamura, M. (2000). Dynamics and Control of a Towed Vehicle in Transient Mode, **International Journal of Offshore and Polar Engineering 10**(1): 19–25.